



**HAL**  
open science

# Porcine reproductive and respiratory syndrome virus degrades TANK-binding kinase 1 via chaperon-mediated autophagy to suppress type I interferon production and facilitate viral proliferation

Shuang-Shuang Zhao, Qisheng Qian, Yao Wang, Songlin Qiao, Rui Li

## ► To cite this version:

Shuang-Shuang Zhao, Qisheng Qian, Yao Wang, Songlin Qiao, Rui Li. Porcine reproductive and respiratory syndrome virus degrades TANK-binding kinase 1 via chaperon-mediated autophagy to suppress type I interferon production and facilitate viral proliferation. *Veterinary Research*, 2024, 55 (1), pp.151. 10.1186/s13567-024-01392-w . hal-04787729

**HAL Id: hal-04787729**

**<https://hal.science/hal-04787729v1>**

Submitted on 18 Nov 2024

**HAL** is a multi-disciplinary open access archive for the deposit and dissemination of scientific research documents, whether they are published or not. The documents may come from teaching and research institutions in France or abroad, or from public or private research centers.


L'archive ouverte pluridisciplinaire **HAL**, est destinée au dépôt et à la diffusion de documents scientifiques de niveau recherche, publiés ou non, émanant des établissements d'enseignement et de recherche français ou étrangers, des laboratoires publics ou privés.

RESEARCH ARTICLE

Open Access



# Porcine reproductive and respiratory syndrome virus degrades TANK-binding kinase 1 via chaperon-mediated autophagy to suppress type I interferon production and facilitate viral proliferation

Shuang-shuang Zhao<sup>1,2</sup>, Qisheng Qian<sup>2</sup>, Yao Wang<sup>2</sup>, Songlin Qiao<sup>2\*</sup> and Rui Li<sup>2\*</sup> 

## Abstract

Porcine reproductive and respiratory syndrome virus (PRRSV) has led to significant economic losses in the global swine industry. Type I interferon (IFN-I) plays a crucial role in the host's resistance to PRRSV infection. Despite extensive research showing that PRRSV employs multiple strategies to antagonise IFN-I induction, the underlying mechanisms remain to be fully elucidated. In this study, we have discovered that PRRSV inhibits the production of IFN-I by degrading TANK-binding kinase 1 (TBK1) through chaperon-mediated autophagy (CMA). From a mechanistic standpoint, PRRSV nonstructural protein 2 (Nsp2) increases the interaction between the heat shock protein member 8 (HSPA8) and TBK1. This interaction leads to the translocation of TBK1 into lysosomes for degradation, mediated by lysosomal-associated membrane protein 2A (LAMP2A). As a result, the downstream activation of IFN regulatory factor 3 (IRF3) and the production of IFN-I are hindered. Together, these results reveal a new mechanism by which PRRSV suppresses host innate immunity and contribute to the development of new antiviral strategies against the virus.

**Keywords** PRRSV, Nsp2, TBK1, IFN-I, CMA

Handling editor: Marie Galloux.

\*Correspondence:

Songlin Qiao  
cdj565@gmail.com

Rui Li  
lirui860620@sina.com

<sup>1</sup> Key Laboratory of Applied Technology On Green-Eco-Healthy Animal Husbandry of Zhejiang Province, Zhejiang Provincial Engineering Laboratory for Animal Health Inspection & Internet Technology, Zhejiang International Science and Technology Cooperation Base for Veterinary Medicine and Health Management, China-Australia Joint Laboratory for Animal Health Big Data Analytics, College of Animal Science and Technology & College of Veterinary Medicine of Zhejiang A&F University, Hangzhou 311300, Zhejiang, China

<sup>2</sup> Institute for Animal Health (Key Laboratory of Animal Immunology), Henan Academy of Agricultural Sciences, Zhengzhou 450002, Henan, China

## Introduction

Innate immunity is the host's first line of defence against RNA viruses [1, 2]. It recognises viral RNAs through pattern recognition receptors and activates IFN regulatory factor 3 (IRF3) or the nuclear factor kappa-light-chain-enhancer of activated B cells (NF- $\kappa$ B)-mediated type I interferon (IFN-I) production [3–6]. The expression of IFN-I is crucial in limiting the early replication and spread of viruses [7]. RNA viruses have developed different mechanisms to suppress innate immunity and establish infection [8].

Porcine reproductive and respiratory syndrome (PRRS) is characterised by severe reproductive failure in sows and respiratory diseases in pigs of all ages. This disease



© The Author(s) 2024. **Open Access** This article is licensed under a Creative Commons Attribution 4.0 International License, which permits use, sharing, adaptation, distribution and reproduction in any medium or format, as long as you give appropriate credit to the original author(s) and the source, provide a link to the Creative Commons licence, and indicate if changes were made. The images or other third party material in this article are included in the article's Creative Commons licence, unless indicated otherwise in a credit line to the material. If material is not included in the article's Creative Commons licence and your intended use is not permitted by statutory regulation or exceeds the permitted use, you will need to obtain permission directly from the copyright holder. To view a copy of this licence, visit <http://creativecommons.org/licenses/by/4.0/>. The Creative Commons Public Domain Dedication waiver (<http://creativecommons.org/publicdomain/zero/1.0/>) applies to the data made available in this article, unless otherwise stated in a credit line to the data.

has imposed a significant economic burden on the global swine industry [9, 10]. Its causative agent, PRRS virus (PRRSV), is a member of the family *Arteriviridae* in the order *Nidovirales*. It is an enveloped, single-stranded positive-sense RNA virus containing a genome of ~15 kb [11, 12]. Two-thirds of the PRRSV genome encodes non-structural proteins (Nsps), including Nsp1 $\alpha$ , Nsp1 $\beta$ , and Nsp2-12, which participate in viral pathogenesis [13–15].

Nsps have been shown to antagonise the host's innate immune responses and facilitate PRRSV persistent infection in vivo (e.g., porcine alveolar macrophages [PAMs]) and in vitro (such as African green monkey kidney cell lines MA-104 and MARC-145) [16–19]. PRRSV Nsp1 $\alpha$ , Nsp4, and Nsp11 all block NF- $\kappa$ B nuclear translocation or eliminate the linear ubiquitination of NF- $\kappa$ B essential modulators, thereby impairing signalling activation and IFN-I production [20–24]. Nsp1 $\beta$  and Nsp2 inhibit the phosphorylation and nuclear translocation of IRF3, which hinders IFN-I expression [25, 26]. Despite these, few studies have previously investigated upstream regulators of IRF3, such as TANK-binding kinase 1 (TBK1).

In this study, we discovered that PRRSV infection leads to the degradation of TBK1. We then identified PRRSV Nsp2 as the factor responsible for TBK1 degradation and outlined the detailed mechanisms involved. Additionally, we found that the degradation of TBK1 by Nsp2 suppresses IRF3-mediated IFN-I production, which in turn facilitates the proliferation of PRRSV.

## Materials and methods

### Cells and viruses

MARC-145, human embryonic kidney 293 T (HEK-293 T), CRL-2843-CD163, and human cervix carcinoma HeLa cells were stored in our laboratory [27]. CRL-2843-CD163 cells were maintained in Roswell Park Memorial Institute 1640 medium (Cat. No. 31800; Solarbio), supplemented with 10% heat-inactivated fetal bovine serum (FBS; Cat. No. 10270-106; Gibco) and antibiotics (100 U/mL penicillin, 100 mg/mL streptomycin; Cat. No. P1400; Solarbio) in a humidified 37 °C and 5% CO<sub>2</sub> incubator. MARC-145 and HEK-293 T cells were maintained in Dulbecco-modified Eagle medium (Cat. No. 12100; Solarbio), supplemented with 10% heat-inactivated FBS and antibiotics. HeLa cells were routinely maintained in modified Eagle medium (Cat. No. 138-0012; iCell Bioscience Inc), supplemented with 10% heat-inactivated FBS and antibiotics at 37 °C in 5% CO<sub>2</sub>.

PRRSV strains HN07-1 (GenBank KX766378.1) and HNhx (GenBank KX766379) were previously isolated by our laboratory [28, 29]. PRRSV strain BJ-4 (GenBank AF331831) was kindly provided by Professor Hanchun

Yang of China Agricultural University. PRRSV strain HN07-1 was utilised in this study unless otherwise stated.

### Antibodies

Rabbit anti-TBK1 monoclonal antibody (mAb; Cat. No. 3504S), rabbit anti-phospho-TBK1 (p-TBK1) mAb (Cat. No. 5483S), rabbit anti-IRF3 mAb (Cat. No. 11904S), rabbit anti-phospho-IRF3 (p-IRF3) mAb (Cat. No. 79945S), rabbit anti-Flag mAb (Cat. No. 14793), mouse anti-myc mAb (Cat. No. 2276S), and rabbit anti-hemagglutinin (HA) mAb (Cat. No. 3724) were all purchased from Cell Signaling Technology. Rabbit anti-heat shock protein member 8 (HSPA8) polyclonal antibodies (pAbs; Cat. No. 10654-1-AP), mouse anti-lysosomal-associated membrane protein 2A (LAMP2A) mAb (Cat. No. 66301-1-Ig), rabbit anti- $\beta$ -actin mAb (Cat. No. 81115-1-RR), and mouse anti-glyceraldehyde-3-phosphate dehydrogenase (GAPDH) mAb (Cat. No. 60004-1-Ig) were purchased from Proteintech. Alexa Fluor 555-goat anti-rabbit IgG pAbs (Cat. No. ab150078), Alexa Fluor 488-goat anti-rabbit IgG pAbs (Cat. No. ab150077), Alexa Fluor 647-goat anti-rabbit IgG pAbs (Cat. No. ab150115), horseradish peroxidase (HRP)-labeled goat anti-rabbit IgG pAbs (Cat. No. ab6721), and HRP-labeled goat anti-mouse IgG pAbs (Cat. No. ab6789) were purchased from Abcam. Rabbit anti-PRRSV nucleocapsid (N) protein pAbs (Cat. No. GTX129270) for immunoblotting (IB) was purchased from GeneTex.

### Reagents

Lipofectamine 2000 (Cat. No. 2066194), Lipofectamine LTX with Plus reagent (Cat. No. 15338030), and Lipofectamine RNAiMAX transfection reagent (Cat. No. 13778150) were purchased from Invitrogen. TransIn-tro<sup>®</sup> PL Transfection Reagent (Cat. No. FT301-01) was purchased from TransGen Biotech. DMSO (Cat. No. 276855), 3-methyladenine (3-MA; Cat. No. M9281), and MG132 (Cat. No. M7449) were purchased from Sigma-Aldrich. Radioimmunoprecipitation assay (RIPA) lysis buffer (Cat. No. P0013B), NP-40 lysis buffer (Cat. No. P0013F), Western blot (WB) /immunoprecipitation (IP) lysis buffer (Cat. No. P0013), fast silver stain kit (Cat. No. P0017S), Triton X-100 (Cat. No. P0096), and 4',6-diamidino-2-phenylindole (DAPI; Cat. No. C1006) were all purchased from Beyotime Biotechnology. 0.25% trypsin-EDTA solution (Cat. No. T1320), phosphate buffered solution (PBS; Cat. No. P1010), and 4% paraformaldehyde (PFA; Cat. No. P1110) were purchased from Solarbio. A complete EDTA-free protease inhibitor cocktail (Cat. No. 04693116001) and universal SYBR green Master (Cat. No. 04913914001) were purchased from Roche. 2 $\times$  loading buffer (Cat. No. 9173), PrimeScript RT master

mix (Cat. No. RR036B), and RNAiso Plus (Cat. No. 9109) were purchased from TaKaRa. Enhanced chemiluminescence (ECL) reagent (Cat. No. P0013B) was purchased from NCM Biotechnology. Chloroquine (CQ; Cat. No. HY-17589A), HA beads (Cat. No. HY-K0201), myc beads (Cat. No. HY-K0206-5), and Flag beads (Cat. No. HY-K0207-5) were purchased from MedChemExpress. PolyI:C (Cat. No. P9582) and 0.22  $\mu\text{m}$  polyvinylidene fluoride membranes (Cat. No. ISEQ00010) were obtained from Sigma-Aldrich. The cell viability assay was performed according to our previous study (data not shown) [30].

### Plasmid constructs and transfection

The gene of each Nsp or Nsp2-mutant from PRRSV strain HN07-1 was synthesised and cloned into the pCAGGS-HA plasmid. Nsp2 from PRRSV strains BJ-4 and HNhx was cloned into the pCAGGS-HA plasmid. The cDNA of TBK1 was constructed into pCMV-3 $\times$ Flag plasmid by GENEWIZ. The full-length HSPA8 was constructed into the pcDNA3.1-myc/his\_A and pEGFP-C1 plasmid by our laboratory [31].

MARC-145, HeLa, and HEK-293 T cells were seeded in cell culture plates and grown to 60~70% confluence for the transfection. Following the manufacturers' instructions, the cells were then transfected with the plasmids using Lipofectamine 2000 or TransIntro PL Transfection Reagent. Unless otherwise specified, 12-well cell culture plates were transfected with 1.5  $\mu\text{g}$  of each plasmid per well, and six-well cell culture plates were transfected with 2.5  $\mu\text{g}$  of each plasmid per well.

### Quantitative real-time PCR (RT-qPCR)

Total RNAs were extracted using TRIzol reagent (Cat. No.15596018; Invitrogen), and then reversely transcribed into cDNA using a PrimeScript RT reagent kit (Cat. No. RR037A) in accordance with the manufacturer's instructions. RT-qPCR amplified the cDNAs from different samples to quantify N abundance using GAPDH mRNA as an endogenous control. The RT-qPCR was performed using a universal SYBR green master on LightCycler480 II (Roche, Basel, Switzerland). The fold change was calculated using the  $2^{-\Delta\Delta\text{CT}}$  method [32]. The primers are listed in Table 1.

### Immunoblotting (IB)

The cells were harvested and then lysed on ice using WB/IP lysis buffer containing a protease inhibitor cocktail. Whole-cell lysates were normalised to equal amounts of GAPDH/ $\beta$ -actin, separated by sodium dodecyl sulfate-polyacrylamide gel electrophoresis (SDS-PAGE), and transferred onto 0.22  $\mu\text{m}$  polyvinylidene fluoride membranes. The membranes were blocked in 5% skimmed

**Table 1** The primers used for RT-qPCR in this study

Primers	Sequence (5'-3')
mon-TBK1-F	CGGAGACCCGGCTGGTATAA
mon-TBK1-R	GCACTAGCTCCTTGGCCATAA
mon-IFN- $\beta$ -F	CTAGCACTGGCTGGAATGAGACT
mon-IFN- $\beta$ -R	GGCCTTCAGTAATGCAGAATC
mon-GAPDH-F	TGACAACAGCCTCAAGATCG
mon-GAPDH-R	GTCTTCTGGGTGGCAGTGAT
pig-HSPA8-F	CGCAGACGTTCCACCACCTAT
pig-HSPA8-R	GGAGGTATGCCCGTGAGTTC
pig-LAMP2-F	GACTGTTTCAGTGTCTGGAGC
pig-LAMP2-R	TCATCCAGCGAACACTCTTGG
pig-IFN- $\beta$ -F	TGCAACCACCACAATTC
pig-IFN- $\beta$ -R	CTGAGAATGCCGAAGATCTG
pig-GAPDH-F	CCTTCGGTGTCCCTACTGCCAAC
pig-GAPDH-R	GACGCCTGCTTACCACCTTCT
N-F	AAACCAGTCCAGAGGCAAGG
N-R	GCAAACATAAACCACAGTGTA

milk at room temperature (RT) for 2 h and then incubated with the primary antibodies at 4  $^{\circ}\text{C}$  overnight. After incubation with the corresponding HRP-conjugated secondary antibodies at RT for 1 h, the IB results were visualised using ECL reagent. Representative images were provided.

### Co-immunoprecipitation (co-IP)

The indicated plasmids were expressed in HEK-293 T cells for 36 h. The cells were lysed with WB/IP lysis buffer containing a protease inhibitor cocktail at 4  $^{\circ}\text{C}$  for 30 min and centrifuged at 12 000  $\times g$  for 10 min. The supernatant was incubated overnight with anti-HA magnetic beads, anti-Flag magnetic beads, or anti-myc magnetic beads at 4  $^{\circ}\text{C}$ . The precipitated immune complexes were collected with a magnetic holder, washed with cold PBS, eluted with a 2 $\times$ loading buffer, and subjected to IB with the indicated antibodies.

### Confocal microscopy

MARC-145 and HeLa cells were transfected with the indicated plasmids or infected with PRRSV for indicated periods. The cells were washed with PBS, fixed with 4% PFA at RT for 10 min, and permeabilised with 0.1% Triton X-100 in PBS at RT for 10 min. After three rinses with cold PBS, the cells were blocked with 5% bovine serum albumin at RT for 1.5 h. After blocking, the cells were incubated overnight with the primary antibodies at 4  $^{\circ}\text{C}$ . After three washes with PBS, the cells were incubated with the appropriate fluorescent secondary antibodies at RT for 1 h. The cell nuclei were stained with DAPI for an additional 5 min. All images were taken and processed using a fluorescence microscope (LSM800, Carl Zeiss AG, Oberkochen, Germany) with a confocal laser scanning setup (20 $\times$ , 40 $\times$ , or 63 $\times$ ). The images represent a

**Table 2** The siRNAs used in this study

Name	Forward sequence (5'-3')	Reverse sequence (5'-3')
siHSPA8(mon)	GGGACAAGGUAUCAAAATT	UUUGAUGAUACCUUGCCCTT
siLAMP2(mon)	GUGGCACUGUGACAUUAATT	UUUAUUGUCACAGUGCCACTT
siHSPA8(pig)	GACCCAGACUUUCACUACUTT	AGUAGUGAAAGUCUGGGUUCTT
siLAMP2(pig)	GGUUACCUCAGUUUAUAUTT	AUUAUAACUGAGGUAACCTT
siNC	UUCUCCGAACGUGUCACGUTT	ACGUGACACGUUCGGAGAATT

single slice from a stack obtained from three independent experiments [33]. The co-localisation analyses were conducted using the JaCoP plugin in ImageJ software following established research guidelines [34–36]. Pearson's correlation coefficient ( $>0.5$ ) describes the correlation of the intensity distribution between channels. Manders' correlation coefficient ( $>0.6$ ) indicates the actual overlap of the signals, representing the true degree of colocalisation [36, 37].

#### HA-IP/mass spectrometry (MS)

HEK-293 T cells were transfected with the plasmid expressing Nsp2-HA or HA-tagged empty vector using Lipofectamine 2000 for 36 h, and then were lysed on ice with WB/IP lysis buffer for 30 min. The cell lysates were centrifuged at  $12\,000\times g$  for 5 min. Anti-HA magnetic beads were incubated overnight with the supernatants at  $4\text{ }^{\circ}\text{C}$ . The beads were washed six times with PBS. The associated proteins were analysed by 12.5% SDS-PAGE, and the protein bands in the gel were stained with a fast silver stain kit. The protein bands were excised and subjected to liquid chromatography and tandem MS (LC-MS/MS) by Lumingbio (Shanghai, China). The top-ranked peptide matches were considered for protein identification, and representative images were displayed.

#### RNA interference

HEK-293 T cells were transfected with small interference RNA (siRNA) targeting HSPA8 (siHSPA8) or LAMP2A (siLAMP2A) using Lipofectamine RNAiMAX according to the manufacturer's instructions at a final concentration of 50 nM for 36 h. For HSPA8 knockdown during PRRSV infection, MARC-145 or CRL-2843-CD163 cells were infected with PRRSV at a multiplicity of infection (MOI) of 1 for 2 h, and then transfected with siHSPA8 or siRNA-negative control (siNC) for 48 h. For LAMP2A knockdown, MARC-145 or CRL-2843-CD163 cells were transfected with siLAMP2A or siNC. At 24 h post-transfection, the cells were infected with PRRSV at an MOI of 1. RT-qPCR or IB detected the knockdown efficiencies. The siRNAs were designed and synthesised by GenePharma (Shanghai, China). The cells were then used for

subsequent experiments. The siRNA sequences are listed in Table 2. The cell viability assay was performed according to our previous study (data not shown) [30].

#### Flow cytometry (FCM)

The MARC-145 cells infected with PRRSV were treated with 0.25% trypsin-EDTA solution, centrifuged at  $2000\times g$ , and re-suspended in PBS. The cells were fixed with 4% PFA, permeabilised with 0.1% Triton X-100, and then blocked with 5% bovine serum albumin. The cells were incubated with or without mouse anti-N mAb at RT for 2 h, and Alexa Fluor 647-goat anti-mouse IgG pAbs at RT for 1 h. Finally, the washed cells were resuspended in PBS and the percentage of PRRSV-infected cells was analysed by a flow cytometer (CytoFLEX; Beckman Coulter, Brea, USA). Representative images were shown.

#### PRRSV titration assay

The PRRSV-infected cells were subjected to three freeze-thaw cycles and centrifuged to collect the supernatant. The progeny virus titers were measured by detecting the 50% tissue culture infected dose (TCID<sub>50</sub>) in MARC-145 cells. In brief, MARC-145 cells were seeded in 96-well cell culture plates and inoculated with a tenfold serial dilution of the supernatant at  $37\text{ }^{\circ}\text{C}$  for 1 h. The excess inoculum was removed by washing it with PBS. The cells were cultured for 3 to 6 days. Cytopathic effects were observed using an inverted microscope (Axiovert 40, Carl Zeiss AG, Oberkochen, Germany). The TCID<sub>50</sub> value was calculated according to the method of Reed-Muench [38].

#### Statistical analysis

Each experiment included three replicates and was independently repeated at least three times. The data are presented as means  $\pm$  standard error of the mean (SEM). Prism 8.0 software (San Diego, USA) performed all data and calculations using the unpaired two-tailed Student *t* test. Statistical significance was represented by asterisks (ns, not significant [ $P>0.05$ ]; \*,  $P<0.05$ ; \*\*,  $P<0.01$ ; \*\*\*,  $P<0.001$ ; \*\*\*\*,  $P<0.0001$ ).

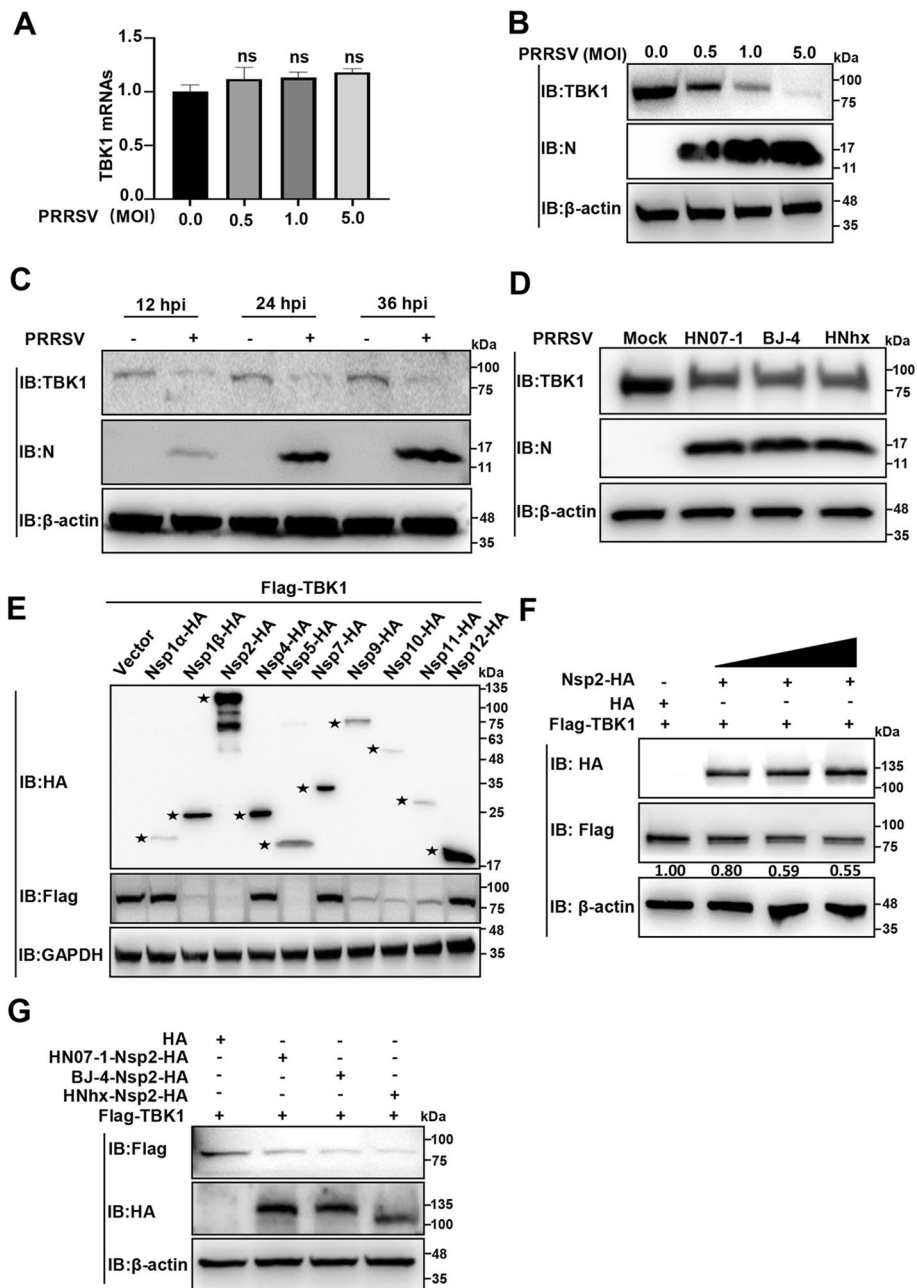


**Figure 1** PRRSV Nsp2 degrades TBK1. **A, B** MARC-145 cells were infected with PRRSV strain HN07-1 at different MOIs (0.5, 1, and 5 MOI) or mock-infected and collected at 24 hpi. **A** The relative TBK1 mRNA abundance was analysed using RT-qPCR. Statistical analysis was carried out using the Student *t* test. ns, not significant ( $P > 0.05$ ) **B** The TBK1 protein abundance was detected using IB. **C** MARC-145 cells were infected with PRRSV strain HN07-1 at an MOI of 1 or mock infected for indicated time periods (12, 24, or 36 h). The TBK1 protein level was detected by IB. **D** The mock-infected, or PRRSV strain HN07-1, BJ-4, or HNhx-infected (MOI = 1) MARC-145 cells were collected at 24 hpi. The TBK1 protein level was detected by IB. **E** HEK-293 T cells were transfected with the plasmids encoding each PRRSV strain HN07-1 Nsp-HA and Flag-TBK1 or HA-tagged empty vector, followed by IB analyses with the specific antibodies. Asterisks mark the target proteins. **F** The Nsp2-HA plasmid (0.5, 1, or 1.5  $\mu$ g) was co-transfected with the Flag-TBK1 plasmid into HEK-293 T cells for 24 h. IB detected the TBK1 protein level. **G** HEK-293 T cells were transfected with the plasmids encoding Nsp2-HA of PRRSV strain HN07-1, BJ-4, or HNhx and Flag-TBK1 or HA-tagged empty vector, followed by IB analyses with the specific antibodies.

## Results

### PRRSV Nsp2 degrades TBK1

Firstly, we examined the RNA and protein levels of endogenous TBK1 in MARC-145 cells infected with the highly pathogenic (HP)-PRRSV strain HN07-1-infected using RT-qPCR and IB. As shown in Figures 1A and 1B, TBK1 RNA levels remained stable, while protein levels decreased significantly in a dose-dependent manner. We observed decreased TBK1 protein levels at 12, 24, and 36 h after HP-PRRSV infection (hpi, Figure 1C). Furthermore, we confirmed that the low pathogenic PRRSV strain BJ-4 and the NADC30-like PRRSV strain HNhx decreased TBK1 abundance (Figure 1D). All these results show that PRRSV infection degrades TBK1.

To identify which PRRSV Nsp2s degraded TBK1, we overexpressed each HA-tagged HP-PRRSV strain HN07-1 Nsp (Nsp-HA) and Flag-tagged-TBK1 (Flag-TBK1) in the HEK-293 T cells, and detected their expression and TBK1 protein levels. As shown in Figure 1E, Nsp1 $\alpha$ -HA, Nsp1 $\beta$ -HA, Nsp2-HA, Nsp4-HA, Nsp5-HA, Nsp7-HA, and Nsp9-12-HA were successfully expressed, and among them, Nsp1 $\beta$ -HA, Nsp2-HA, Nsp5-HA, and Nsp9-11-HA degraded TBK1. As our laboratory has been investigating Nsp2 [39], we have proceeded with further research focusing on Nsp2-induced degradation of TBK1. We observed that the overexpression of HP-PRRSV Nsp2-HA led to a reduction in the abundance of exogenous TBK1 in a manner that depended on the dosage (Figure 1F). We verified that the Nsp2-HA of PRRSV strains BJ-4 and HNhx reduced TBK1 protein levels (Figure 1G). These data demonstrate that PRRSV Nsp2 degrades TBK1.

### PRRSV Nsp2 interacts with TBK1 and induces its degradation via lysosomal pathway

We next examined whether PRRSV Nsp2 interacted with TBK1. We co-transfected the Nsp2-HA and Flag-TBK1 plasmids into HEK-293 T cells and performed IP using anti-HA/Flag magnetic beads. As shown in Figure 2A, we detected an interaction between exogenous Nsp2-HA and Flag-TBK1. Meanwhile, we overexpressed Nsp2-HA and Flag-TBK1 in HeLa cells and observed their co-localisation via confocal microscopy. Their co-localisation was further quantified using Pearson's correlation coefficient, and the mean value was 0.745, indicating an interaction between these two proteins (Figure 2B). In addition, we monitored that endogenous Nsp2 interacted with TBK1 by IP and confocal microscopy in the PRRSV-infected MARC-145 cells (Figures 2C, D). These results substantiate that PRRSV Nsp2 specifically interacts with TBK1.

Considering their interaction, we initially assessed whether Nsp2 directly degrades TBK1. The PRRSV Nsp2 cysteine protease domain possesses both trans- and

cis-cleavage activities, with highly conserved C55, C111, H124, C142, and C147 being responsible for the activities [40]. We mutated these residues to alanine (named Nsp2-mutant-HA) and detected that Nsp2-mutant-HA still degraded TBK1 (Figure 2E), indicating that its degradation was independent of Nsp2 cysteine protease activity. As the autolysosomal pathway and ubiquitin-proteasome system are two main host cellular degradation routes [41, 42], we investigated whether PRRSV Nsp2 degrades TBK1 through these two routes using the autophagy inhibitor 3-MA, lysosomal inhibitor CQ, and the proteasome inhibitor MG132 [43–45]. As shown in Figure 2F, only CQ treatment reversed TBK1 degradation, suggesting that Nsp2 induces TBK1 degradation in a lysosome-dependent manner.

### PRRSV Nsp2 interacts with HSPA8

To understand how Nsp2 breaks down TBK1 using lysosomes, we screened the host cellular proteins targeted by PRRSV Nsp2. We used IP along with LC-MS/MS. In cells overexpressing Nsp2-HA, we observed a distinct protein band marked by a red arrow (~71 kDa), identified as HSPA8 (Figure 3A).

To confirm that Nsp2 interacted with HSPA8, we co-transfected the Nsp2-HA and HSPA8-myc plasmids in HEK-293 T cells and detected an interaction between exogenous Nsp2 and HSPA8 (Figure 3B). Furthermore, we overexpressed Nsp2-HA and HSPA8-myc in HeLa cells and observed their co-localisation via confocal microscopy (Figure 3C). Moreover, we conducted IP and confocal microscopy in the PRRSV-infected cells and monitored endogenous Nsp2 interacting with HSPA8 (Figures 3D, E). These data indicate that PRRSV Nsp2 specifically interacts with HSPA8.

### PRRSV Nsp2 degrades TBK1 via chaperone-mediated autophagy (CMA)

HSPA8 recognises the Lys-Phe-Glu-Arg-Gln (KFERQ) motif on target proteins and forms HSPA8-substrate complexes; the complexes are subsequently translocated into lysosomes via LAMP2A for degradation, namely CMA [46]. It has been reported that HSPA8 interacts with TBK1 and degrades it via CMA [47]. Therefore, we hypothesised that Nsp2 enhances the interaction between HSPA8 and TBK1 to promote its degradation. We detected that Nsp2-HA overexpression strengthened the interaction of HSPA8-myc with Flag-TBK1 (Figures 4A, B). We also found that TBK1 localisation in lysosomes increased in PRRSV-infected MARC-145 cells (the Manders' correlation coefficient increased from 0.617 to 0.889, Figure 4C). We then applied siHSPA8 or

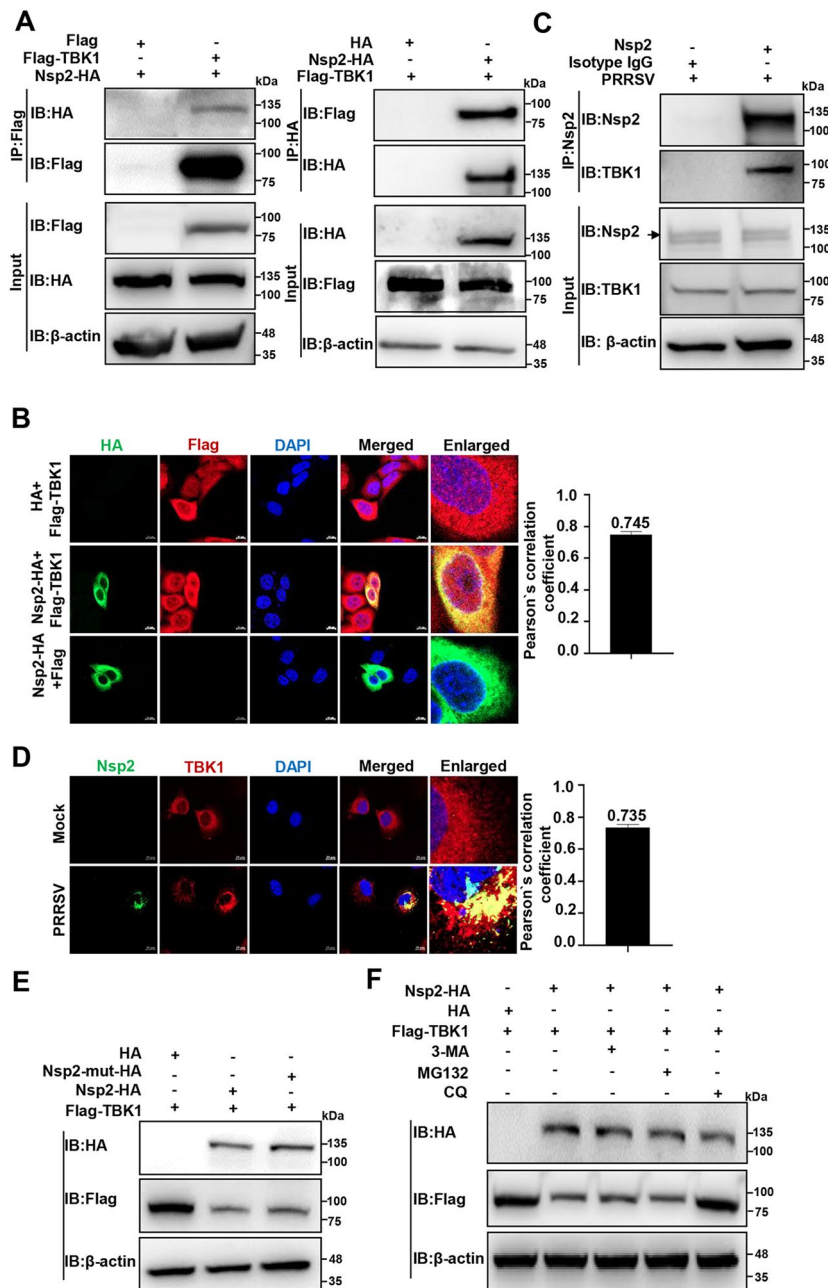


**Figure 2** PRRSV Nsp2 interacts with TBK1 and induces its degradation via the lysosomal pathway. **A** HEK-293 T cells were transfected with the plasmids encoding Nsp2-HA and Flag-TBK1 or HA/Flag-tagged empty vector for 36 h, followed by co-IP with anti-HA/Flag magnetic beads and IB analyses with anti-HA/Flag antibodies. **B** HeLa cells were transfected with the plasmids encoding Nsp2-HA and Flag-TBK1 for 24 h. In parallel, HeLa cells were transfected with the plasmid encoding Nsp2-HA and Flag-tagged empty vector, or Flag-TBK1 and HA-tagged empty vector. Flag-TBK1 and Nsp2-HA were visualised with the specific primary and secondary antibodies. Cell nuclei were stained with DAPI. The fluorescent signals were observed with confocal microscopy (scale bars = 10 μm). The co-localisation was assessed by determination of the Pearson's correlation coefficient using the JaCoP plugin in ImageJ software. **C** MARC-145 cells were infected with PRRSV at an MOI of 1 for 24 h. They were then analysed via endogenous IP using protein A/G magnetic beads pre-incubated with anti-Nsp2 pAbs, and IB with anti-Nsp2 and anti-TBK1 antibodies. **D** MARC-145 cells were infected with PRRSV at an MOI of 0.1 for 24 h. The fluorescent signals were observed with confocal microscopy (scale bars = 10 μm). The co-localisation was assessed by determining the Pearson's correlation coefficient using the JaCoP plugin in ImageJ software. **E** HEK-293 T cells were co-transfected with the plasmids encoding Flag-TBK1 and Nsp2-HA or Nsp2-mutant-HA. At 24 h post-transfection, the cell lysates were collected to analyse the TBK1 protein level with IB. **F** HEK-293 T cells were transfected with the plasmids encoding Nsp2-HA and Flag-TBK1 for 6 h. 3-MA, CQ, MG132, or DMSO was added and the samples were collected after 24 h for IB analyses with anti-HA and anti-Flag antibodies.



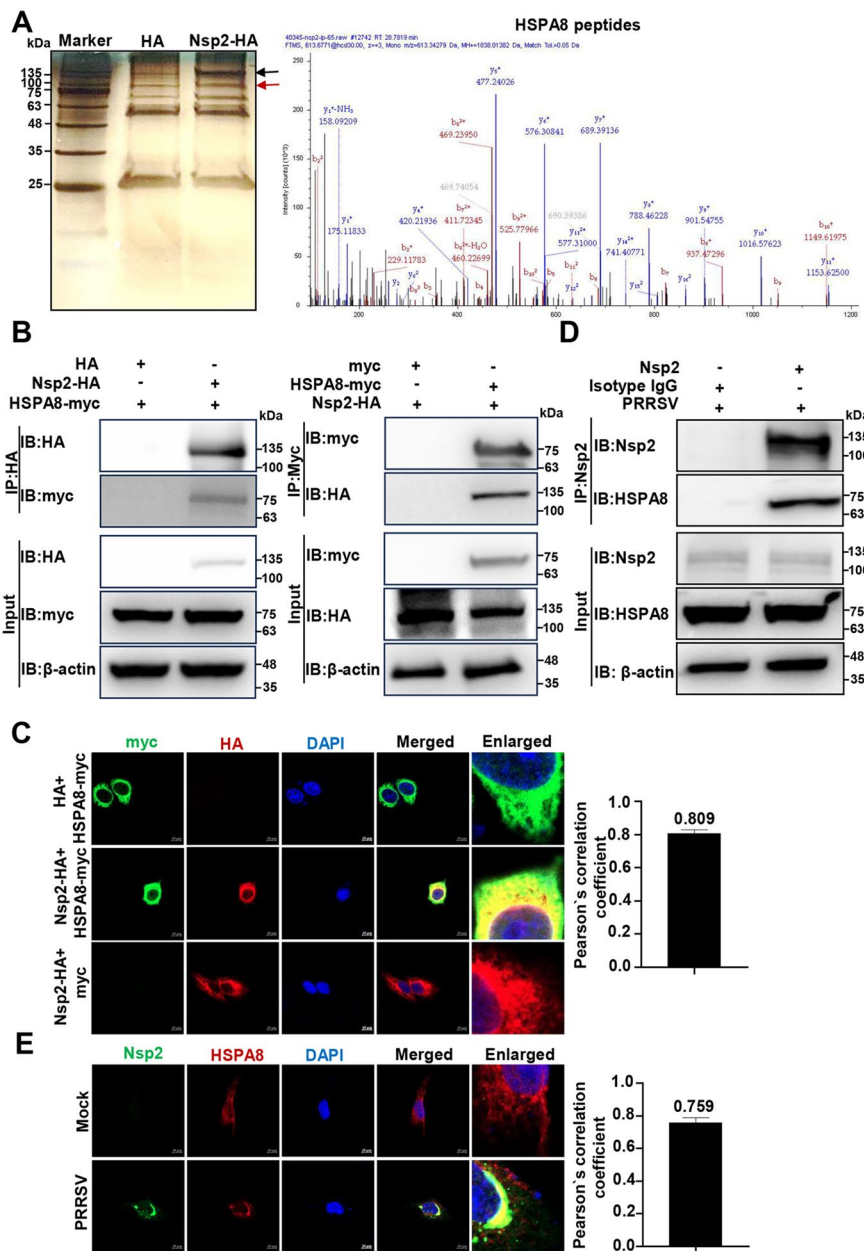


**Figure 3** PRRSV Nsp2 interacts with HSPA8. **A** HEK-293 T cells were transfected with the plasmid expressing HA or Nsp2-HA. The proteins were immunoprecipitated in cell lysates using an anti-HA antibody, separated by 12% SDS-PAGE, and stained with silver. The red arrow indicates the significantly different immunoprecipitated protein band. The black arrow marks Nsp2-HA. The panel on the right shows the tandem MS analysis of HSPA8 peptides. **B** HEK-293 T cells were transfected with the plasmids encoding Nsp2-HA and HSPA8-myc or HA/myc-tagged empty vector for 36 h, followed by co-IP with anti-HA or anti-myc magnetic beads, and IB analyses with anti-HA and anti-myc antibodies. **C** HeLa cells were transfected with the plasmids encoding Nsp2-HA and HSPA8-myc for 24 h. In parallel, HeLa cells were transfected with the plasmid encoding Nsp2-HA and myc-tagged empty vector, or HSPA8-myc and HA-tagged empty vector. HSPA8-myc and Nsp2-HA were visualised with the specific primary and secondary antibodies. Cell nuclei were stained with DAPI. The fluorescent signals were observed with confocal microscopy (scale bars = 10 μm). The co-localisation was assessed by determination of the Pearson's correlation coefficient using the JaCoP plugin in ImageJ software. **D** MARC-145 cells were infected with PRRSV at an MOI of 1 for 24 h. They were then analysed via endogenous IP using protein A/G magnetic beads pre-incubated with anti-Nsp2 pAbs, and IB with anti-Nsp2 and anti-HSPA8 antibodies. **E** MARC-145 cells were infected with PRRSV at an MOI of 1 for 24 h. The fluorescent signals were observed with confocal microscopy (scale bars = 10 μm). The co-localisation was assessed by determination of the Pearson's correlation coefficient using the JaCoP plugin in ImageJ software.

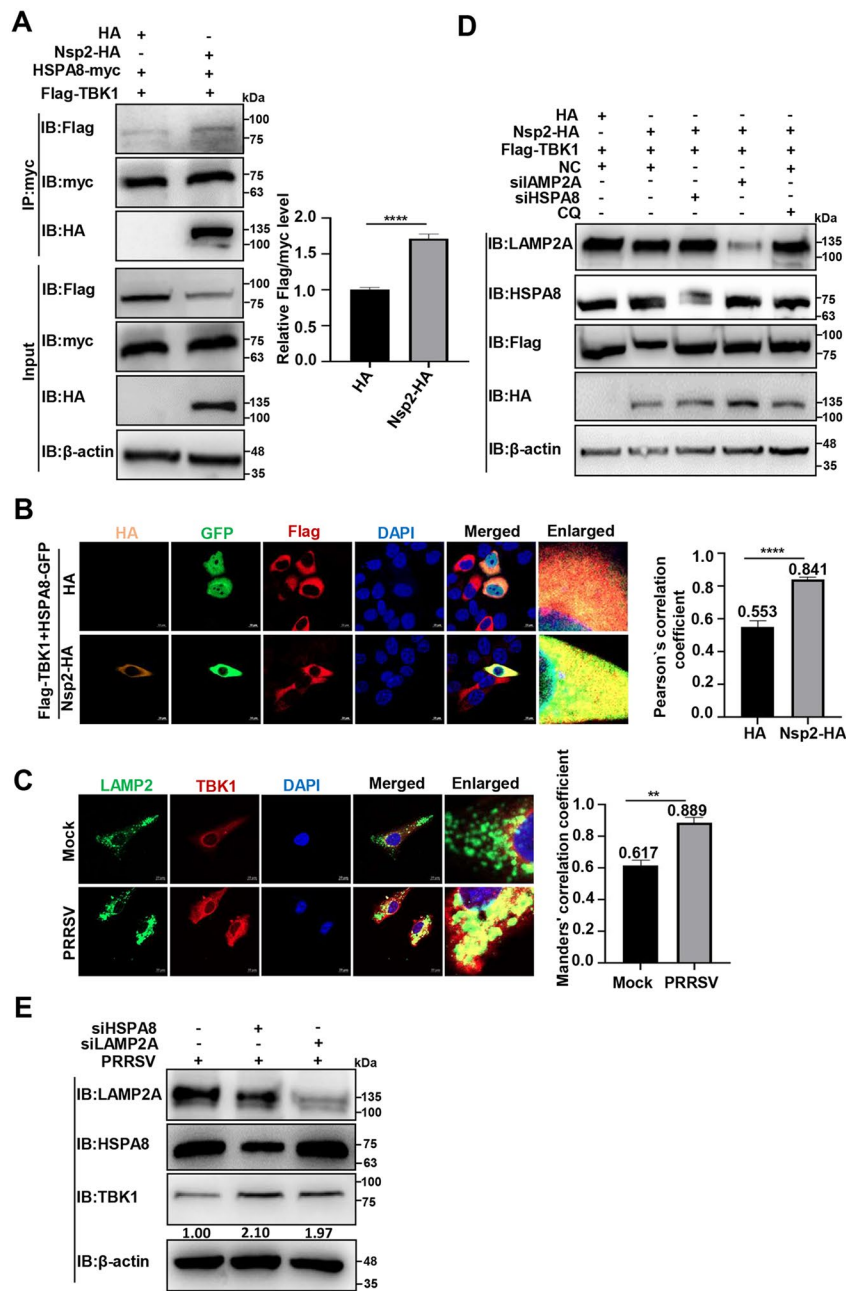


**Figure 4** PRRSV Nsp2 degrades TBK1 via CMA. **A** HEK-293 T cells were transfected with the plasmids encoding Flag-TBK1, HSPA8-myc, and Nsp2-HA or HA-tagged empty vector for 36 h. Co-IP was performed with anti-myc magnetic beads and IB was conducted with the specific antibodies. **B** HeLa cells were transfected with the plasmids encoding Flag-TBK1, HSPA8-myc, and Nsp2-HA or HA-tagged empty vector for 36 h. The fluorescent signals were observed with confocal microscopy. The co-localisation was assessed by determination of the Pearson's correlation coefficient (scale bars = 10 μm) using the JaCoP plugin in ImageJ software. **C** MARC-145 cells were infected with PRRSV at 0.1 MOI for 24 h. The fluorescent signals were observed with confocal microscopy. The co-localisation was assessed by determination of the Manders' correlation coefficient (scale bars = 10 μm) using the JaCoP plugin in ImageJ software. **D** HEK-293 T cells were transfected with siHSPA8, siLAMP2A, or siNC, and the plasmids encoding Flag-TBK1 and Nsp2-HA. The samples were collected after 36 h for IB analyses with the specific antibodies. **E** MARC-145 cells were transfected with siHSPA8/LAMP2A or siNC to detect their effects during PRRSV infection, and IB was conducted with the specific antibodies. The data are presented as means ± SEM from three independent experiments. Statistical analysis was carried out using the Student *t* test. \*\*,  $P < 0.01$ , \*\*\*\*,  $P < 0.0001$ .

siLAMP2A and found that the knockdown of HSPA8 and LAMP2A reversed TBK1 degradation by Nsp2-HA (Figure 4D). Similarly, TBK1 degradation was antagonised during PRRSV infection in the *HSPA8* and *LAMP2A* knockdown cells (Figure 4E). Taken together, these data provide evidence that Nsp2 degrades TBK1 via CMA.

**PRRSV Nsp2 degrades TBK1 via CMA to suppress IRF3 activation and IFN production**

TBK1 activates IRF3 signalling and initiates IFN production [48]. Consequently, we speculated that TBK1 degradation by Nsp2 via CMA hampered the p-TBK1 level, thereby hindering p-IRF3 levels and IFN production. As expected, overexpression of Nsp2-HA decreased the TBK1, p-TBK1, and p-IRF3 levels (Figure 5A). In contrast, the knockdown of HSPA8 and LAMP2A reversed the Nsp2-HA-induced degradation of TBK1 and

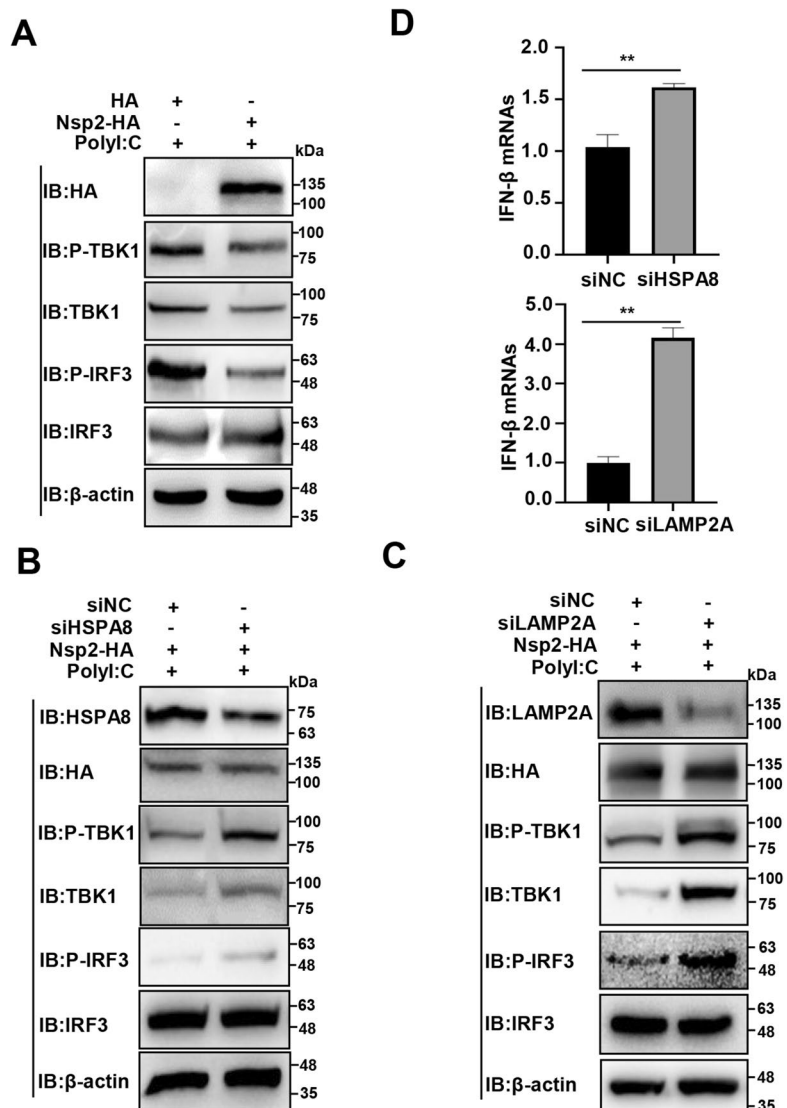


**Figure 5** PRRSV Nsp2 degrades TBK1 via CMA to suppress IRF3 activation and IFN production. **A** HEK-293 T cells were transfected with the plasmid encoding Nsp2-HA or HA-tagged empty vector. The PolyI:C was added 12 h before the sample was collected. IB was conducted with the specific antibodies. **B, C** HEK-293 T cells were transfected with siHSPA8, siLAMP2A, or siNC, and the plasmid encoding Nsp2-HA. The PolyI:C was added 12 h before the sample was collected. IB was conducted with the specific antibodies. **D** HEK-293 T cells were transfected with siHSPA8, siLAMP2A, or siNC, and the plasmid encoding Nsp2-HA. The PolyI:C was added 12 h before the sample was collected. IFN-β RNA abundance was detected using RT-qPCR. The data are presented as means ± SEM from three independent experiments. Statistical analysis was carried out using the Student *t* test. \*\*, *P* < 0.01.

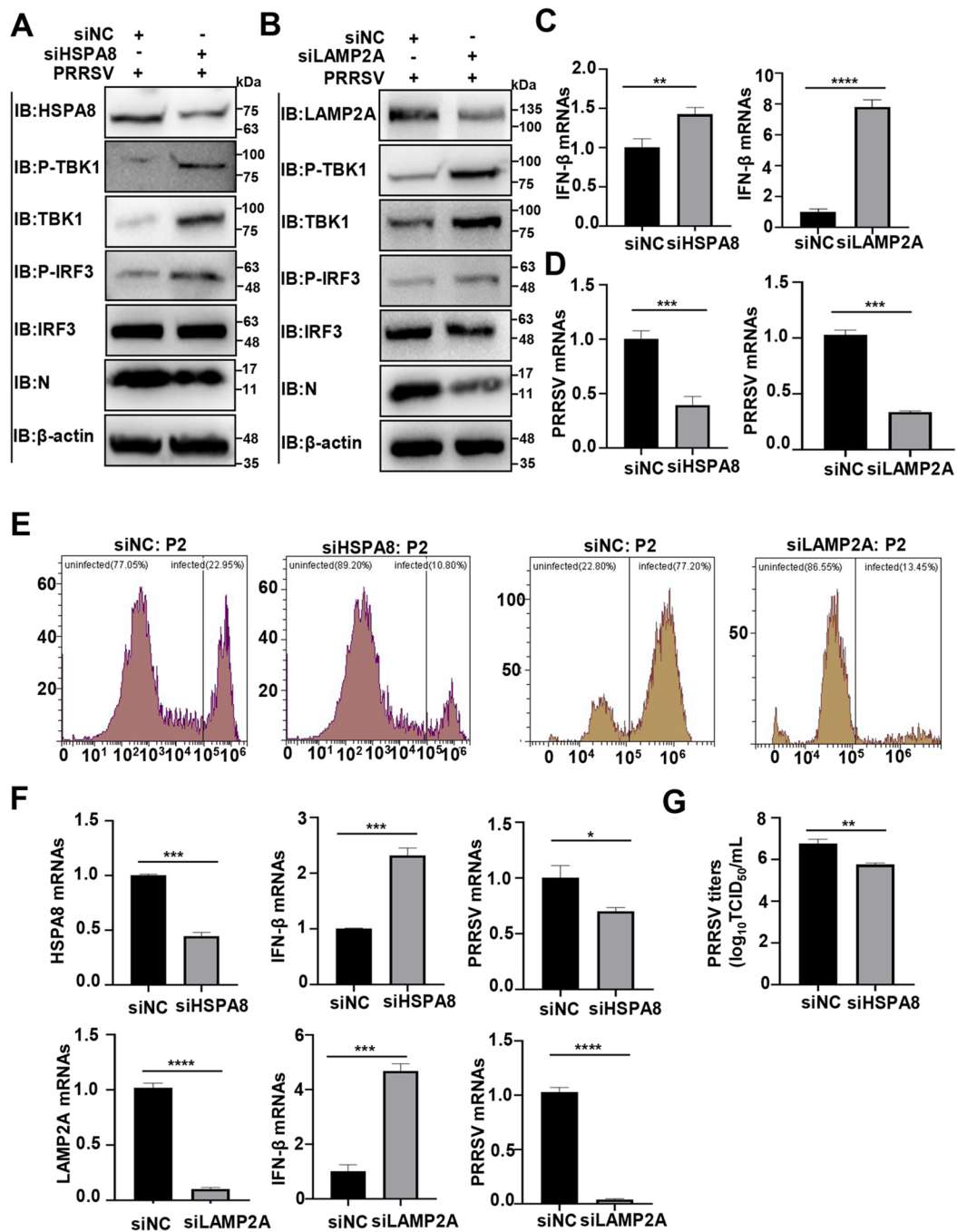


**Figure 6** PRRSV degrades TBK1 via CMA to suppress innate immunity and facilitate viral proliferation. **A** MARC-145 cells were infected with PRRSV at an MOI of 1 for 2 h, then transfected with siHSPA8 or siNC for 48 h, and IB was conducted with the specific antibodies. **B** MARC-145 cells were transfected with siLAMP2A or siNC for 24 h. At 24 h post-transfection, the cells were infected with PRRSV at an MOI of 1 and IB was conducted with the specific antibodies. **C–E** MARC-145 cells were transfected with siHSPA8/siLAMP2A or siNC to detect their effects during PRRSV infection. **C** IFN- $\beta$  RNA abundance was detected using RT-qPCR. **D** PRRSV RNA abundance was detected using RT-qPCR. **E** PRRSV infection was detected using FCM. **F** CRL-2843-CD163 cells were transfected with siHSPA8/siLAMP2A and the cell lysates were collected to detect their effects during PRRSV infection. IFN- $\beta$  RNA and PRRSV RNA abundance were detected using RT-qPCR. **G** CRL-2843-CD163 cells were transfected with siHSPA8 or siNC. PRRSV titers were measured by assessing TCID<sub>50</sub>. The data are presented as means  $\pm$  SEM from three independent experiments. Statistical analysis was carried out using the Student t test. \*,  $P < 0.05$ ; \*\*,  $P < 0.01$ ; \*\*\*,  $P < 0.0011$ ; \*\*\*\*,  $P < 0.0001$ .

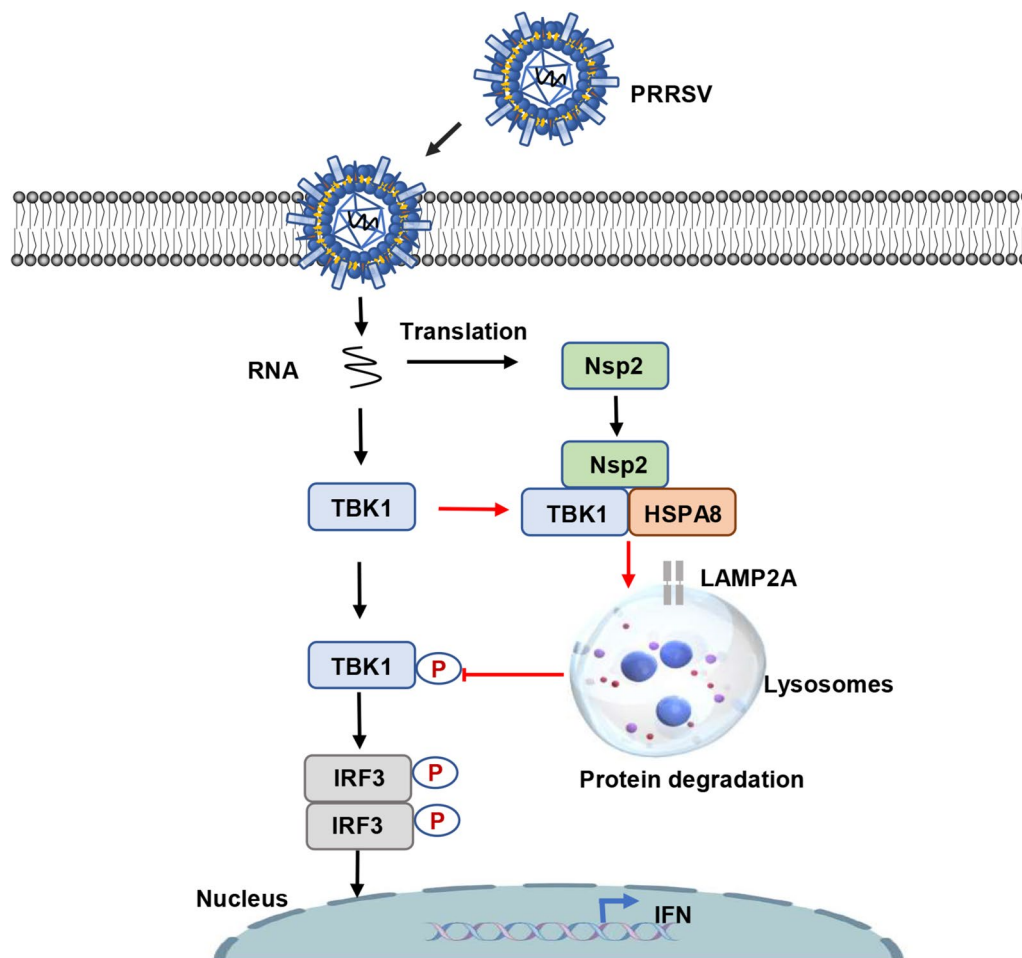


**Figure 7** Schematic model depicting that PRRSV inhibits IFN-I production by degrading TBK1 via CMA, thereby promoting viral proliferation. Mechanistically, PRRSV Nsp2 enhances the interaction between HSPA8 and TBK1, leading to LAMP2A-mediated translocation of TBK1 into lysosomes for degradation, which impedes downstream IRF3 signalling and IFN-I production.

increased the p-TBK1 and p-IRF3 levels (Figures 5B, C). Additionally, *HSPA8* and *LAMP2A* knockdown enhanced IFN- $\beta$  production (Figure 5D). These data show that PRRSV Nsp2 degrades TBK1 through CMA to inhibit IRF3 activation and IFN production.

#### PRRSV degrades TBK1 via CMA to suppress innate immunity and promote viral proliferation

We further investigated the impact of PRRSV-induced TBK1 degradation via CMA on the host's innate immunity and viral proliferation. Figures 6A, B show that the knockdown of *HSPA8/LAMP2A* enhanced the TBK1, p-TBK1, and p-IRF3 levels during PRRSV infection. Meanwhile, *HSPA8/LAMP2A* knockdown increased IFN- $\beta$  mRNA abundance while decreasing PRRSV RNA

levels, as detected by RT-qPCR (Figures 6C, D). FCM results also showed that intracellular PRRSV infection was lowered (~50% reduction in the *HSPA8* knockdown cells and ~80% reduction in the *LAMP2A* knockdown ones, Figure 6E). As PAMs are primary *in vivo* target cells for PRRSV infection, we further performed the assays in a continuous PAM cell line CRL-2843-CD163, which stably expresses PRRSV indispensable receptor CD163 [49, 50]. Similarly, siHSPA8/siLAMP2A increased IFN- $\beta$  RNA abundance and decreased PRRSV RNA levels (Figure 6F). The knockdown of *HSPA8* also reduced PRRSV titres by at least tenfold ( $>1 \log_{10} \text{TCID}_{50} \text{ mL}^{-1}$ , Figure 6G). These results show that PRRSV degrades TBK1 through CMA to suppress innate immunity and facilitate viral proliferation.

## Discussion

PRRSV employs various strategies to suppress innate immunity and establish persistent infection, posing a major obstacle to PRRS eradication [14]. Therefore, it is crucial to understand the interaction between PRRSV and the host's innate immunity to elucidate PRRSV pathogenesis and improve prevention and control strategies. PRRSV Nsp2 antagonises the host's innate immune responses [51]. However, there are limited studies on their antagonism of TBK1-mediated IFN production.

TBK1 is a kinase that mediates innate immune signaling. TBK1 phosphorylation leads to downstream IRF3 activation and IFN-I responses [52, 53], and is strictly regulated by several mechanisms [48, 54]. For example, the E3 ubiquitin ligase DTX4 promotes the polyubiquitination of TBK1 at Lys670 with K48 linkage, resulting in TBK1 degradation and the inhibition of immune responses [55].

In this study, we observed that different PRRSV strains degrade TBK1, and we further identified that PRRSV Nsp2 degrades TBK1 (Figure 1). Nsp2 carries out papain-like cysteine protease activities and cleaves viral polyproteins to produce Nsp2s as well as other target proteins for PRRSV replication [39, 40]. Interestingly, we found that PRRSV Nsp2 interacted with TBK1 but degraded TBK1 independent of its cysteine protease activity (Figure 2). Subsequently, we showed that PRRSV Nsp2 degrades TBK1 via CMA, which reveals a new mechanism for protein degradation by Nsp2.

CMA is a form of selective autophagy, where proteins containing the KFERQ motif are recognised by HSPA8 and then translocated into lysosomes via LAMP2A for degradation [46]. It has been shown to participate in TBK1 degradation [47]. We confirmed that PRRSV Nsp2 interacts with HSPA8 and enhances its interaction with TBK1 to degrade TBK1 via CMA (Figures 3 and 4).

Finally, PRRSV Nsp2-induced TBK1 degradation via CMA decreased TBK1 phosphorylation levels and inhibited downstream IRF3 activation. This suppressed IFN-I production and promoted viral proliferation (Figures 5 and 6). PRRSV Nsp2 is well-known for its involvement in immunosuppression [26, 56–58]. In detail, Nsp2 impedes the transport of stimulator of IFN genes from the endoplasmic reticulum to the Golgi apparatus and blocks IFN signalling [56]. In addition, Nsp2 inhibits the signalling of melanoma differentiation-associated gene 5, which impairs immune responses [57]. Nsp2 also antagonises NF- $\kappa$ B-mediated immune responses by deubiquitinating K48-linked I- $\kappa$ B- $\alpha$  [58]. Moreover, Nsp2 prevents the phosphorylation and nuclear translocation of IRF3, thereby reducing the expression of IFN-I [26]. Our study reveals a different mechanism through which Nsp2 suppresses the host's innate immunity.

Based on these results, we propose a model to describe how PRRSV degrades TBK1 via CMA to suppress host innate immunity and facilitate viral proliferation (Figure 7). Our results contribute to a comprehensive understanding of PRRSV immunosuppression and provide promising targets for the prevention and control of PRRS.

## Abbreviations

PRRSV	porcine reproductive and respiratory syndrome virus
IFN-I	type I interferon
TBK1	TANK-binding kinase 1
CMA	chaperon-mediated autophagy
Nsp2	nonstructural protein 2
HSPA8	heat shock protein member 8
LAMP2A	lysosomal-associated membrane protein 2A
IRF3	IFN regulatory factor 3
NF- $\kappa$ B	nuclear factor kappa-light-chain-enhancer of activated B cells
PRRS	porcine reproductive and respiratory syndrome
PAMs	porcine alveolar macrophages
HEK-293 T	human embryonic kidney 293 T
FBS	fetal bovine serum
mAb	monoclonal antibody
p-TBK1	phospho-TBK1
p-IRF3	phospho-IRF3
HA	hemagglutinin
pAbs	polyclonal antibodies
GAPDH	glyceraldehyde-3-phosphate dehydrogenase
HRP	horseradish peroxidase
N	nucleocapsid
IB	immunoblotting
RIPA	radioimmunoprecipitation assay
WB/IP	Western blot/immunoprecipitation
DAPI	4',6-Diamidino-2-phenylindole
ECL	enhanced chemiluminescence
RT-qPCR	quantitative real-time PCR
SDS-PAGE	sodium dodecyl sulfate–polyacrylamide gel electrophoresis
RT	room temperature
MS	mass spectrometry
LC–MS/MS	liquid chromatography and tandem MS
siRNA	small interference RNA
MOI	multiplicity of infection
siNC	siRNA-negative control
FCM	flow cytometry
TCID <sub>50</sub>	50% Tissue culture infected dose
SEM	standard error of the mean
hpi	hours post-infection

## Acknowledgements

We thank Professor Hanchun Yang from China Agricultural University for providing PRRSV strain BJ-4.

## Authors' contributions

RL and SQ jointly supervised the work. S-SZ and RL designed the experiments. S-SZ performed the studies. S-SZ and RL analysed the data. QQ and YW provided technical assistance. S-SZ wrote the manuscript. S-SZ, RL, and SQ revised the manuscript. All authors read and approved the final manuscript.

## Funding

This study was supported by grants from the National Natural Science Foundation of China (32272993 and 32172875), the Program for Central Plains Youth Top Talent, and the Special Fund for Henan Agriculture Research System (HARS-22–12-S).

## Availability of data and materials

The data generated during this study are available from the corresponding authors upon reasonable request.

## Declarations

### Competing interests

The authors declare that they have no competing interests.

Received: 15 April 2024 Accepted: 27 August 2024

Published online: 14 November 2024

## References

- Müller U, Steinhoff U, Reis LF, Hemmi S, Pavlovic J, Zinkernagel RM, Aguet M (1994) Functional role of type I and type II interferons in antiviral defense. *Science* 264:1918–1921
- Sadler AJ, Williams BR (2008) Interferon-inducible antiviral effectors. *Nat Rev Immunol* 8:559–568
- O'Neill LA, Bowie AG (2010) Sensing and signaling in antiviral innate immunity. *Curr Biol* 20:R328–333
- Liu G, Gack MU (2020) Distinct and orchestrated functions of RNA sensors in innate immunity. *Immunity* 53:26–42
- Hiscott J (2007) Triggering the innate antiviral response through IRF-3 activation. *J Biol Chem* 282:15325–15329
- Hiscott J, Grandvaux N, Sharma S, Tenover BR, Servant MJ, Lin R (2003) Convergence of the NF- $\kappa$ B and interferon signaling pathways in the regulation of antiviral defense and apoptosis. *Ann NY Acad Sci* 1010:237–248
- Stetson DB, Medzhitov R (2006) Type I interferons in host defense. *Immunity* 25:373–381
- Chathuranga K, Weerawardhana A, Dodantenna N, Lee JS (2021) Regulation of antiviral innate immune signaling and viral evasion following viral genome sensing. *Exp Mol Med* 53:1647–1668
- Valdes-Donoso P, Jarvis LS (2022) Combining epidemiology and economics to assess control of a viral endemic animal disease: Porcine Reproductive and Respiratory Syndrome (PRRS). *PLoS One* 17:e0274382
- Lunney JK, Benfield DA, Rowland RR (2010) Porcine reproductive and respiratory syndrome virus: an update on an emerging and re-emerging viral disease of swine. *Virus Res* 154:1–6
- Dokland T (2010) The structural biology of PRRSV. *Virus Res* 154:86–97
- Conzelmann KK, Visser N, Van Woensel P, Thiel HJ (1993) Molecular characterization of porcine reproductive and respiratory syndrome virus, a member of the arterivirus group. *Virology* 193:329–339
- Fang Y, Snijder EJ (2010) The PRRSV replicase: exploring the multifunctionality of an intriguing set of nonstructural proteins. *Virus Res* 154:61–76
- Lunney JK, Fang Y, Ladinig A, Chen N, Li Y, Rowland B, Renukaradhya GJ (2016) Porcine reproductive and respiratory syndrome virus (PRRSV): pathogenesis and interaction with the immune system. *Annu Rev Anim Biosci* 4:129–154
- Music N, Gagnon CA (2010) The role of porcine reproductive and respiratory syndrome (PRRS) virus structural and non-structural proteins in virus pathogenesis. *Anim Health Res Rev* 11:135–163
- Kim HS, Kwang J, Yoon IJ, Joo HS, Frey ML (1993) Enhanced replication of porcine reproductive and respiratory syndrome (PRRS) virus in a homogeneous subpopulation of MA-104 cell line. *Arch Virol* 133:477–483
- Duan X, Nauwynck HJ, Pensaert MB (1997) Virus quantification and identification of cellular targets in the lungs and lymphoid tissues of pigs at different time intervals after inoculation with porcine reproductive and respiratory syndrome virus (PRRSV). *Vet Microbiol* 56:9–19
- Duan X, Nauwynck HJ, Pensaert MB (1997) Effects of origin and state of differentiation and activation of monocytes/macrophages on their susceptibility to porcine reproductive and respiratory syndrome virus (PRRSV). *Arch Virol* 142:2483–2497
- Wills RW, Doster AR, Galeota JA, Sur JH, Osorio FA (2003) Duration of infection and proportion of pigs persistently infected with porcine reproductive and respiratory syndrome virus. *J Clin Microbiol* 41:58–62
- Song C, Krell P, Yoo D (2010) Nonstructural protein 1 $\alpha$  subunit-based inhibition of NF- $\kappa$ B activation and suppression of interferon- $\beta$  production by porcine reproductive and respiratory syndrome virus. *Virology* 407:268–280
- Huang C, Zhang Q, Guo XK, Yu ZB, Xu AT, Tang J, Feng WH (2014) Porcine reproductive and respiratory syndrome virus nonstructural protein 4 antagonizes beta interferon expression by targeting the NF- $\kappa$ B essential modulator. *J Virol* 88:10934–10945
- Chen J, Wang D, Sun Z, Gao L, Zhu X, Guo J, Xu S, Fang L, Li K, Xiao S (2019) Arterivirus nsp4 antagonizes interferon beta production by proteolytically cleaving NEMO at multiple sites. *J Virol* 93:e00385-19
- Wei ZY, Liu F, Li Y, Wang HL, Zhang ZD, Chen ZZ, Feng WH (2020) Aspartic acid at residue 185 modulates the capacity of HP-PRRSV nsp4 to antagonize IFN- $\beta$  expression. *Virology* 546:79–87
- Su Y, Shi P, Zhang L, Lu D, Zhao C, Li R, Zhang L, Huang J (2018) The superimposed deubiquitination effect of OTULIN and porcine reproductive and respiratory syndrome virus (PRRSV) Nsp11 promotes multiplication of PRRSV. *J Virol* 92:e00175-18
- Beura LK, Sarkar SN, Kwon B, Subramaniam S, Jones C, Pattnaik AK, Osorio FA (2010) Porcine reproductive and respiratory syndrome virus nonstructural protein 1 $\beta$  modulates host innate immune response by antagonizing IRF3 activation. *J Virol* 84:1574–1584
- Li H, Zheng Z, Zhou P, Zhang B, Shi Z, Hu Q, Wang H (2010) The cysteine protease domain of porcine reproductive and respiratory syndrome virus non-structural protein 2 antagonizes interferon regulatory factor 3 activation. *J Gen Virol* 91:2947–2958
- Liu Y, Li R, Chen XX, Zhi Y, Deng R, Zhou EM, Qiao S, Zhang G (2019) Nonmuscle myosin heavy chain IIA recognizes sialic acids on sialylated RNA viruses to suppress proinflammatory responses via the DAP12-syk pathway. *MBio* 10:e00574-19
- Qiao S, Feng L, Bao D, Guo J, Wan B, Xiao Z, Yang S, Zhang G (2011) Porcine reproductive and respiratory syndrome virus and bacterial endotoxin act in synergy to amplify the inflammatory response of infected macrophages. *Vet Microbiol* 149:213–220
- Wang LJ, Wan B, Guo Z, Qiao S, Li R, Xie S, Chen XX, Zhang G (2018) Genomic analysis of a recombinant NADC30-like porcine reproductive and respiratory syndrome virus in china. *Virus Genes* 54:86–97
- Zheng XX, Li R, Qiao S, Chen XX, Zhang L, Lu Q, Xing G, Zhou EM, Zhang G (2021) Vimentin rearrangement by phosphorylation is beneficial for porcine reproductive and respiratory syndrome virus replication in vitro. *Vet Microbiol* 259:109133
- Wang L, Li R, Geng R, Zhang L, Chen XX, Qiao S, Zhang G (2022) Heat shock protein member 8 (HSPA8) is involved in porcine reproductive and respiratory syndrome virus attachment and internalization. *Microbiol Spectr* 10:e0186021
- Schmittgen TD, Livak KJ (2008) Analyzing real-time PCR data by the comparative C(T) method. *Nat Protoc* 3:1101–1108
- Wei X, Li R, Qiao S, Chen XX, Xing G, Zhang G (2020) Porcine reproductive and respiratory syndrome virus utilizes viral apoptotic mimicry as an alternative pathway to infect host cells. *J Virol* 94:e00709-20
- Zinchuk V, Grossenbacher-Zinchuk O (2009) Recent advances in quantitative colocalization analysis: focus on neuroscience. *Prog Histochem Cytochem* 44:125–172
- Bolte S, Cordelières FP (2006) A guided tour into subcellular colocalization analysis in light microscopy. *J Microsc* 224:213–232
- Dunn KW, Kamocka MM, McDonald JH (2011) A practical guide to evaluating colocalization in biological microscopy. *Am J Physiol Cell Physiol* 300:C723-742
- Jensen EC (2013) Quantitative analysis of histological staining and fluorescence using ImageJ. *Anat Rec (Hoboken)* 296:378–381
- Reed LJ, Muench H (1938) A simple method of estimating fifty per cent endpoints. *Am J Epidemiol* 27:493–497
- Ss Z, Qian Q, Chen Xx LuQ, Xing G, Qiao S, Li R, Zhang G (2024) Porcine reproductive and respiratory syndrome virus triggers Golgi apparatus fragmentation-mediated autophagy to facilitate viral self-replication. *J Virol* 98:e0184223
- Han J, Rutherford MS, Faaberg KS (2009) The porcine reproductive and respiratory syndrome virus nsp2 cysteine protease domain possesses both trans- and cis-cleavage activities. *J Virol* 83:9449–9463
- Mizushima N, Komatsu M (2011) Autophagy: renovation of cells and tissues. *Cell* 147:728–741
- Wang Y, Le WD (2019) Autophagy and ubiquitin-proteasome system. *Adv Exp Med Biol* 1206:527–550
- Wu YT, Tan HL, Shui G, Bauvy C, Huang Q, Wenk MR, Ong CN, Codogno P, Shen HM (2010) Dual role of 3-methyladenine in modulation of

- autophagy via different temporal patterns of inhibition on class I and III phosphoinositide 3-kinase. *J Biol Chem* 285:10850–10861
44. Guo N, Peng Z (2013) MG132, a proteasome inhibitor, induces apoptosis in tumor cells. *Asia Pac J Clin Oncol* 9:6–11
  45. Ferreira PMP, Sousa RWR, Ferreira JRO, Militão GCG, Bezerra DP (2021) Chloroquine and hydroxychloroquine in antitumor therapies based on autophagy-related mechanisms. *Pharmacol Res* 168:105582
  46. Cuervo AM, Wong E (2014) Chaperone-mediated autophagy: roles in disease and aging. *Cell Res* 24:92–104
  47. Zhao X, Di Q, Yu J, Quan J, Xiao Y, Zhu H, Li H, Ling J, Chen W (2022) USP19 (ubiquitin specific peptidase 19) promotes TBK1 (TANK-binding kinase 1) degradation via chaperone-mediated autophagy. *Autophagy* 18:891–908
  48. Liu S, Cai X, Wu J, Cong Q, Chen X, Li T, Du F, Ren J, Wu YT, Grishin NV, Chen ZJ (2015) Phosphorylation of innate immune adaptor proteins MAVS, STING, and TRIF induces IRF3 activation. *Science* 347:aaa2630
  49. Lee YJ, Park CK, Nam E, Kim SH, Lee OS, du Lee S, Lee C (2010) Generation of a porcine alveolar macrophage cell line for the growth of porcine reproductive and respiratory syndrome virus. *J Virol Methods* 163:410–415
  50. Xu YL, Wu SP, Li YG, Sun FX, Wang QJ, Zhao Q, Yu J, Tian FL, Wu JQ, Zhu RL, Peng J (2020) A porcine alveolar macrophage cell line stably expressing CD163 demonstrates virus replication and cytokine secretion characteristics similar to primary alveolar macrophages following PRRSV infection. *Vet Microbiol* 244:108690
  51. Chen XX, Qiao S, Li R, Wang J, Li X, Zhang G (2023) Evasion strategies of porcine reproductive and respiratory syndrome virus. *Front Microbiol* 14:1140449
  52. Fitzgerald KA, McWhirter SM, Faia KL, Rowe DC, Latz E, Golenbock DT, Coyle AJ, Liao SM, Maniatis T (2003) IKKepsilon and TBK1 are essential components of the IRF3 signaling pathway. *Nat Immunol* 4:491–496
  53. Al Hamrashdi M, Brady G (2022) Regulation of IRF3 activation in human antiviral signaling pathways. *Biochem Pharmacol* 200:115026
  54. Deng M, Tam JW, Wang L, Liang K, Li S, Zhang L, Guo H, Luo X, Zhang Y, Petrucelli A, Davis BK, Conti BJ, June Brickey W, Ko CC, Lei YL, Sun S, Ting JP (2020) TRAF3IP3 negatively regulates cytosolic RNA induced anti-viral signaling by promoting TBK1 K48 ubiquitination. *Nat Commun* 11:2193
  55. Cui J, Li Y, Zhu L, Liu D, Songyang Z, Wang HY, Wang RF (2012) NLRP4 negatively regulates type I interferon signaling by targeting the kinase TBK1 for degradation via the ubiquitin ligase DTX4. *Nat Immunol* 13:387–395
  56. Diao F, Bai J, Jiang C, Sun Y, Gao Y, Nauwynck H, Jiang P, Liu X (2023) The papain-like protease of porcine reproductive and respiratory syndrome virus impedes STING translocation from the endoplasmic reticulum to the Golgi Apparatus by deubiquitinating STIM1. *J Virol* 97:e0018823
  57. Zhu Z, Zhang M, Yuan L, Xu Y, Zhou H, Lian Z, Liu P, Li X (2023) LGP2 promotes type I interferon production to inhibit PRRSV infection via enhancing MDA5-mediated signaling. *J Virol* 97:e0184322
  58. Sun Z, Chen Z, Lawson SR, Fang Y (2010) The cysteine protease domain of porcine reproductive and respiratory syndrome virus nonstructural protein 2 possesses deubiquitinating and interferon antagonism functions. *J Virol* 84:7832–7846

## Publisher's Note

Springer Nature remains neutral with regard to jurisdictional claims in published maps and institutional affiliations.